IEEE Access
Multidisciplinary : Rapid Review : Open Access Journal

Received 19 May 2022, accepted 6 July 2022, date of publication 12 July 2022, date of current version 18 July 2022.

Digital Object Identifier 10.1109/ACCESS.2022.3190078

APPLIED RESEARCH

A Kalman Filter-Based Protection Strategy for Microgrids

FAISAL MUMTAZ[1], KASHIF IMRAN[1], SYED BASIT ALI BUKHARI[2], KHAWAJA KHALID MEHMOOD[2], ABDULLAH ABUSORRAH[3], (Senior Member, IEEE), MAQSOOD AHMAD SHAH[1], AND SYED ALI ABBAS KAZMI[1]

[1]USPCAS-E, National University of Sciences and Technology (NUST), Islamabad 44000, Pakistan
[2]Department of Electrical Engineering, University of Azad Jammu and Kashmir, Muzaffarabad 13100, Pakistan
[3]Department of Electrical and Computer Engineering, King Abdulaziz University, Jeddah 21589, Saudi Arabia

Corresponding author: Kashif Imran (kashifimran@uspcase.nust.edu.pk)

Deanship of Scientific Research (DSR) in King Abdul-Aziz University, Jeddah, Saudi Arabia, has funded this project, under grant no. (RG-6-135-38).

ABSTRACT Recently, the concept of microgrids has emerged in the world due to the integration of distributed energy resources (DERs) at the distribution end. The design of a reliable protection strategy is one of the top-most challenges associated with microgrids. This is because of the transition of microgrids between grid-tied and autonomous modes of operation. This paper presents a state-of-the-art microgrid protection scheme based on the Kalman filter (KF). The proposed scheme uses the one-end current signal of a distribution line for the detection and classification of faults. Firstly, the KF is applied to each phase of a three-phase current signal individually to generate residuals and total harmonic distortion (THDs). Next, the variations in the residuals and THDs of each phase are compared with pre-specified threshold values to detect the faulty events in the microgrid. As each phase is processed through KF individually, therefore, the proposed scheme is inherently phase segregated. Afterward, the KF is applied to extract the third harmonic component from the three-phase current and voltage signals. Then, the KF-based reactive power (KFBRP) is obtained from the extracted third harmonic components. Finally, the directional properties of the three-phase KFBRP are used to locate the faulty section in the microgrids. Extensive simulations in MATLAB/Simulink software are performed for the grid-tied as well as the autonomous modes of operation under radial and meshed topologies. The results show that the proposed scheme is highly robust in all testing scenarios without any false tripping and blinding issues.

INDEX TERMS Fault-detection, fault location, high-impedance fault, Kalman filter, microgrid protection scheme, state estimation.

I. INTRODUCTION

Micro-grids are properly designed, controlled and protected systems, which consist of distributed energy resources (DERs), storage devices, and electrical loads. Micro-grids can operate in; (i) an autonomous mode with inverter interfaced DER (IIDER); (ii) an autonomous mode with synchronous-based DER (SDER); and (iii) grid-tied mode. This multi-mode operation of a micro-grid is accompanied by various protection and control challenges [1], [2].

The protection of microgrids is challenging due to the different fault current characteristics in different operating modes [3]. More precisely, the fault current in the autonomous mode of operation is considerably low about 2 to 3 times the rated current of the system, whereas the fault current in grid-tied mode is significantly high. Furthermore, the bidirectional flows of power make the protection more challenging. Traditional overcurrent relays, which are based on the assumption of single-mode operation and high fault current, cannot protect the microgrids in all operating modes [4], [5]. Therefore, there is a need for a microgrid protection strategy that guarantees protection in both the grid-tied and autonomous mode of operation [6].

The associate editor coordinating the review of this manuscript and approving it for publication was Sarasij Das.

Several protection schemes for microgrids have been proposed in the literature. The authors in [7], suggested an adaptive protection strategy for microgrid, which used a digital relay and a central controller to upgrade the relay setting in consequence to the microgrid operating mode. This strategy was further improved in [8] by presenting an online method for calculating the relay setting. In [9], Elbana *et al.* presented a smart protection scheme that used a micro-phasors measurement unit (PMUs) to measure the data at various locations of the microgrid. A microgrid central controller used the measured data to perform various protection functions. The authors in [10] suggested a dynamic adaptive protection scheme by using adaptive overcurrent relaying. An adaptive protection scheme has been suggested for the distribution network with electronically linked DERs in [11]. This scheme monitored the system and upgraded the relay fault current setting according to system variation during a fault condition. Zarei *et al.*in [12], presented a voltage-restrained negative-sequence resistance-based protection strategy for inverter-based microgrids. The authors in [13], used a short-time Fourier transform to obtain the voltage signal features. These features were then provided to a decision tree (DT) to classify fault and no-fault conditions in the microgrid. In [14], Manditereza and Bansal presented a voltage-based microgrid protection strategy by using a relay with a power and sensitivity analysis algorithm. Reference [15] used voltage sag, current magnitude, and active power flow to protect the inverter-based microgrid. In [16], the authors proposed a differential protection scheme by using the injection of off-nominal frequencies through voltage-frequency control of inverter-based microgrids.

In [17], an autocorrelation function-based microgrid protection scheme was presented. The scheme used low pass filtering and squaring law approach to detect and classify the faults in microgrids. In [18], the authors presented a protection scheme that used time-time (TT) transform to detect, locate and classify the faults. It also required a large communication infrastructure. In [19], a Teager-Kaiser energy operator for analyzing the current signal from one end of the considered line is presented to detect and classify the faults in microgrids. The authors in [20] used Hilbert-transform-based superimposed components and reactive energy to protect the microgrids. In [21], wavelet transform was utilized to detect locate and classify the faults in a looped microgrid. In [22] and [23], the authors presented microgrid protection schemes based on positive-sequence components by using PMUs and central processing units (CPU).

Recently, some intelligent methods have also been used to protect the microgrid against different kinds of faults. In [24], an interval type-2 fuzzy logic method was used to detect, locate, and classify the microgrids' faults. A TT-transform and a deep belief network were used for the protection of microgrids [25]. The authors proposed a data mining-based differential microgrid protection scheme [26]. The authors in [27] suggested a combined wavelet and data mining-based approach for microgrid protection. In [28], the support vector machine (SVM) classifier detected the existence of a fault in the microgrid. The strategies presented in [29] and [30] used a convolutional neural network to protect the microgrids. KF was used for microgrids protection in [31] for islanding detection based on the harmonic signature. KF was also used for incipient fault detection in underground cables [32]. In addition, KF was also used for state estimation and microgrid control in [33]. A novel events detection and classification strategy was proposed in [34], using KF algorithm. Although the above-mentioned strategies tried to solve the microgrid protection problem in various aspects, they have some limitations. The majority of these schemes depend on network architecture and are designed for the radial topologies and not intended for looped or meshed topologies. Moreover, only a few of the schemes have considered high impedance faults (HIF).

In this study, a KF-based microgrid protection scheme is proposed. First, the three-phase current signal is measured at the terminal of each distribution line in the microgrid. Next, the KF is employed on each phase of the three-phase current signal separately to obtain the residuals and THDs. Then, the variation in the residuals and THDs are compared with pre-specified threshold values to detect and classify the fault events in a microgrid. Afterward, the third harmonic components of voltage and current signals are extracted by using KF, which are then used to obtain the KF-based reactive power. Finally, the faulty section in the microgrid is identified by using the directional characteristics of the three-phase reactive power. Several simulations have been performed in the MATLAB/Simulink software package to test the validity of the proposed protection scheme. The results show that the presented scheme can detect, classify and locate faults in a microgrid efficiently and quickly. The contributions of the proposed scheme are as follows;

1. First-time utilization of KF in both frequency/time domains for fault detection, classification, and localization in AC microgrids.
2. A reliable criterion for fault-detection and classification is developed, which is independent of fault type and is valid for all types of faults including HIF and low impedance faults.
3. The proposed scheme is valid for both grid-tied and autonomous modes in radial and meshed topologies of microgrids.
4. The scheme can protect microgrids against solid as well as high impedance faults (HIF).
5. The proposed scheme can also protect the microgrids under noisy measurement conditions.

The structure of the remaining paper is as follows: Section II describes the basic mathematical modeling of the proposed protection scheme. The proposed scheme is explained in Section III. Section IV illustrates the standard International Electro-Technical Commission (IEC) Microgrid test model. Simulation results are presented in Section V. Finally, section VII concludes the paper.

II. MATHEMATICAL MODELLING

A. LINEARIZED DYNAMIC SYSTEM MODEL

In the proposed scheme, a real-time KF-based strategy is used for microgrid protection. The proposed scheme uses only the current signal to detect and classify the faults. Furthermore, both current and voltage signals are used for fault location. The microgrid is a non-linear dynamic balanced three-phase system with non-sinusoidal and noisy current and voltage signals during the fault. The single-phase representation of the current and voltage signals in a microgrid is as follows.

$$I_n = M_n \cos(\omega_0 n + \phi) \tag{1}$$

$$V_n = M_n \cos(\omega_0 n + \phi) \tag{2}$$

where, I_n and V_n represent the current and voltage signals of phase A at the nth sample, respectively. The remaining two phases (b and c) will be simply ± 120 degrees apart from phase A. M_n and ϕ denote the amplitude of the measured signal and noise, respectively. The angular frequency $\omega_\circ$ can be calculated using $\omega_\circ = 2\pi \left(f_\circ / f_s\right)$.

Where; $f_\circ$ is the fundamental frequency of the power system. A similar model is adopted for the current and voltage signals, so, only the modeling of current is discussed here. The trigonometric derivative of eq **(1)** results in an iterative equation, which is given as follows.

$$I_{n+1} + I_{n-1} = 2M_n \cos(\omega_0) I_n + w_n \tag{3}$$

where w_n represents an expected zero mean arbitrary error. A single-phase current signal, in terms of the measurement noise and other arbitrary noises, is denoted by zero means (u_n), which is given as follows;

$$i_n = I_n + u_n \tag{4}$$

A state-space representation of the above non-linear dynamic system as a linearized noisy current signal is as follows;

$$\hat{X}_{n+1} = \boldsymbol{A} x_n + b w_n \tag{5}$$

$$i_n = H x_n + u_n \tag{6}$$

where;

x_n System states; $\hat{X}_n = \begin{bmatrix} I_n & I_{n-1} \end{bmatrix}^{-1}$; $b = \begin{bmatrix} 1 & 0 \end{bmatrix}^T$;
$H = \begin{bmatrix} 1 & 0 \end{bmatrix}^T$; $\quad \boldsymbol{A} = \begin{bmatrix} 2\cos\omega_\circ & -1 \\ 1 & 0 \end{bmatrix}$

In the presence of faults, eq's **(5)**, and **(6)** will have some measurement noise. By using the above two equations and iterative equations of KF in APPENDIX, the fundamental and non-fundamental components of current can be estimated. The fundamental current components of each phase are used to calculate the residuals, whereas the non-fundamental components of current are used to calculate THD. The non-fundamental components are estimated by replacing the term $\omega_\circ$ with $h\omega_\circ$ in Matrix $\boldsymbol{A}$. Where $h \; \varepsilon \; N$ represents the order of harmonics in the system (N= 2,3,5,7...). The dynamic system does not depend on the term $\omega_\circ$ and, $h\omega_\circ$, and convergence of KF is not influenced by these terms $\omega_\circ$ and $h\omega_\circ$.

B. KALMAN FILTER

The Kalman Filter is an important tool for analyzing a wide range of estimation problems. Optimal state estimation of electrical magnitudes can be done from a set of their noisy linearized sampled values in a very short interval and by considering only a few samples. KF has a very small computational burden as compared to other estimation techniques. It is an efficient iterative process with three main steps: (i) the calculation of Kalman gain K_G; (ii) the calculation of the current estimate; and (iii) the calculation of new error in the estimate. The operation of the KF propagates through the calculation of mean and covariance over time. The iterative process of KF stops when the updated or new estimate becomes close to the real value or in other words, a new error in the estimate becomes close to zero [31].

C. RESIDUAL'S AND THD'S CALCULATION

The intermittent nature of DERs introduces uncertainty in fault current levels. Moreover, the fault current magnitude is different in each operating scenario due to the limited current carrying capability of power electronics devices. As a result, fault detection is challenging in microgrids. As a result, fault detection is challenging in microgrids. In this paper, KF-based dual criteria have been developed to detect and classify the fault. The criteria are based on the residuals and THDs of each phase of the current signal. The proposed fault-detection criteria can successfully detect and classify the solid and HIF faults in all operating modes of a microgrid.

The residual of the *nth* sample can be calculated by taking the difference between the estimated output current signal to the predicted output current signal.

$$R_{kf}(n) = i_n(p) - i_n(e) \tag{7}$$

where;

$R_{kf}(n)$: Residual of *nth* sample.
$i_n(e)$: *nth* sample of the estimated output current signal
$i_n(p)$: *nth* sample of the predicted output current signal.

The estimated non-fundamental components of current are used for the calculation of THD. The THD can be expressed as follows;

$$\text{THD} = \frac{i_h}{i_f} \tag{8}$$

where;

i_h= Total signal harmonics = $\sqrt{i_2^2 + i_3^2 + \ldots + i_n^2}$
i_n = RMS value of harmonics
i_f =RMS value of fundamental current.

D. KFBRP CHARACTERISTICS DURING FAULT

To design an appropriate and generalized protection scheme, each distribution line (DL) within a microgrid is separately protected. The proposed scheme uses the directional properties of the KFBRP for the location of faults in the microgrid. The KFBRP can be calculated as follows:

$$Q_F = 3V_F * I_F \sin(\Phi_F) \tag{9}$$

where, Q_n represents the instantaneous three-phase KFBRP at the *nth* sample, where the Φ_F represents the angle difference between post-fault voltage and current at the *nth* sample.

$$\Phi_F = \angle V_F - \angle I_F \tag{10}$$

FIGURE 1, elaborates the first simulated three-bus test system for the conceptualization of the directional properties of KFBRP during forward fault (F-1), and Reverse fault ' (F-2). Whereas, the operating direction of the Reference relay (R_R) is assumed from B-1 to B-3.

1) KFBRP DURING F-1

The direction of power flow during forward faults F-1 is the same in direction as the R_R, as shown in FIGURE 1 (a). However, the main assumptions [34];

$$\left\{ \begin{array}{l} v\angle 0; for\ the\ main\ grid\ (MG) \\ v\angle \delta; for\ distributed\ generation \end{array} \right\} \tag{11}$$

Therefore, the estimated pre-fault voltage signals at *nth* sample of bus-2 were given as follows;

$$V_{F1} = V_M \sin(\omega_0 t + \Phi_{F1}) \tag{12}$$

whereas, after the occurrence of F-1 the superimposed voltage and current are calculated as follows;

$$(L_{12} + L_{2F1}) \frac{\partial i_{2F1}(t)}{\partial i_{2F1}(t)} = -\Delta V_{2F1} = V_M \sin(\omega_0 t + \Phi_{F1}) \tag{13}$$

Meanwhile, the L_{12}, and L_{2F} upstream equivalent inductances of line 1 to 2, and line 2 to F_1 [20].

$$I_{2F1}(t) = \frac{V_M}{L_{12} + L_{2F1}} (\cos(\Phi_{F1}) - \cos(\omega_0 t + \Phi_{F1})) \tag{14}$$

$$V_{2F1}(t) = -(L_{12}) \frac{\partial i_{2F}(t)}{\partial i_{2F}(t)} = -\frac{L_{12}}{L_{12} + L_{2F1}} V_M \sin(\omega_0 t + \Phi_{F1}) \tag{15}$$

Therefore, the post-fault voltage is reversed, and the three-phase KFBRP estimated by KF during F-1 is computed as;

$$\hat{Q_{F1}} = -3V_{2F1} * I_{2F1} sin(\Phi_{F1}) \tag{16}$$

Hence, the vector multiplication of the negative angle of post-fault voltage and positive angle of the estimated third harmonics of current signals at the *nth* sample results in the negative 3-phase KFBRP as depicted in FIGURE 1(c).

2) KFBRP DURING F-2

However, during the Reverse faults F-2, the post-fault current phase angle is the same, as shown in FIGURE 1 (b). Conversely, the post-fault assumptions;

$$\left\{ \begin{array}{l} v\angle \delta; for\ the\ main\ grid (MG) \\ v\angle 0; for\ distributed\ generation \end{array} \right\} \tag{17}$$

As during reverse fault the post-fault superimposed voltage [20], [35]; and current are calculated as follows;

$$(L_{2F2} + L_{23} + L_3) \frac{\partial i_{2F2}(t)}{\partial i_{2F2}(t)} = \Delta V_{2F2} = -V_M \sin(\omega_0 t + \Phi_{F2}) \tag{18}$$

However, L_{2F2}, L_{23}, and L_3 upstream equivalent inductances of line 2 to 3, and line 2 to F-2.

So,

$$I_{2F2}(t) = \frac{V_M}{L_{2F2} + L_{23} + L_3} (\cos(\omega_0 t + \Phi_{F2}) - \cos(\Phi_{F2})) \tag{19}$$

$$V_{2F2}(t) = -\frac{L_{23} + L_3}{L_{2F2} + L_{23} + L_3} V_M \sin(\omega_0 t + \Phi_{F1}) \tag{20}$$

Therefore, the three-phase KFBRP during F-2 is computed as follows;

$$\hat{Q_{F2}} = 3V_{2F2} * I_{2F2} sin(\Phi_{F2}) \tag{21}$$

Hence, [20] the vector multiplication of the positive angle of post-fault current and positive angle of the post-fault voltage signals at the *nth* sample results in the positive 3-phase KFBRP as depicted in FIGURE 1 (d). In summary, it is concluded from eqs **(16)**, and **(21)**, that the value of the KFBRP will be negative for forward faults, whereas the value of KFBRP will be positive for reverse faults.

E. THRESHOLD SETTING

An accurate threshold value is necessary to avoid protection blinding and false tripping problems. The proposed approach uses the residuals and THDs of each phase to detect and classify the faults in the microgrid. For a healthy system, the residuals and the THDs for all phases should be zero. However, in practical, due to noisy data, the presence of harmonics, and continuous load change, the residual and the THD have a small non-zero value. To calculate the threshold values for the residual and the THD, extensive simulations have been performed under healthy but worst conditions. As a result, a value of 0.3 for both the residuals and the THDs is obtained. Therefore, if the values of either the residuals or the THDs of any phase become higher than this value, then the system was regarded as in the fault condition. All types of faults are precisely and timely detected and classified in grid-tied and autonomous modes under radial or meshed scenarios by using these threshold values.

III. PROPOSED PROTECTION SCHEME

The schematic diagram of the proposed scheme is shown in FIGURE 2. The proposed scheme consists of five modules: data acquisition, state estimation, fault detection and classification, fault location, and isolation modules. The working of each of the modules has been presented in the following subsections.

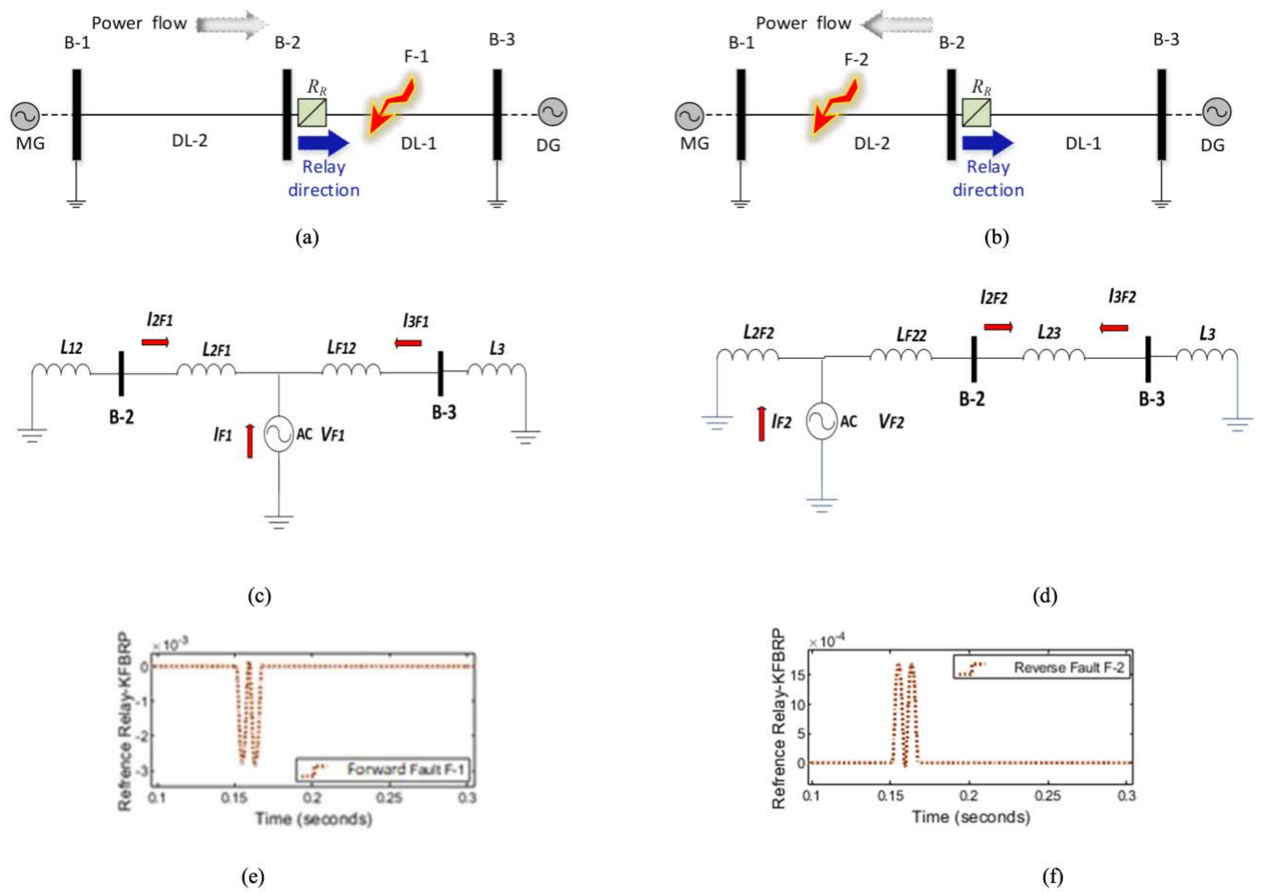

FIGURE 1. First simulated 3- Bus test system, (a) Forward fault case, (b) Reverse fault case, (c) F-1 case Equivalent circuit, (d) F-2 case Equivalent circuit (e) KFBRP during F-1, (f) KFBRP during F-2.

A. DATA ACQUISITION MODULE

This module retrieves and preprocesses the three-phase voltage and current signals at both terminals of a line to be protected. An analog-to-digital converter (ADC) of 12 bits with a 3.6 kHz sampling frequency is used to transform the measured analog signal into the digital signal. A second-order low pass Bessel filter with a cut-off frequency of 1600 Hz is used as an antialiasing filter. The antialiasing filter is used to remove higher frequency components from the input signal to avoid the aliasing effect. The obtained discrete signal is then used as input to the KF for feature extraction.

B. STATE ESTIMATION MODULE

In this module, the KF is applied to each phase individually to extract features from the current and voltage signal in different operating scenarios. The estimated/predicted fundamental component and non-fundamental components of current signals are extracted by separately applying KF to each phase. The extracted components are then used as an input to the fault-detection/classification module at the next stage. The third harmonic components are extracted from the three-phase voltage signals, which are used in the fault-location module to locate the faults in microgrids.

C. FAULT-DETECTION/CLASSIFICATION MODULE

The fault-detection/classification (FDC) module is the main unit in the proposed protection scheme. The FDC module performs its operation in two stages.

In the first stage, the residuals and the THDs from the extracted fundamental and non-fundamental current components are calculated. The residuals are obtained by taking the difference of the fundamental components of estimated and predicted currents by using the eq (7). The THD is calculated by using eq (**8**).

In the second stage, the obtained residuals and the THDs of each phase are compared with a pre-defined threshold value to check the occurrence of faults. If the values of residuals or the THDs of any phase are more than the pre-defined threshold values, the system is considered to have a fault. The proposed microgrid protection scheme is inherently phase segregated; therefore, an additional fault classification module is not required.

D. COMMUNICATION-ASSISTED FAULT-LOCATION MODULE

To accelerate the system restoration and to scale down the outage time, an exact fault location is necessary. The

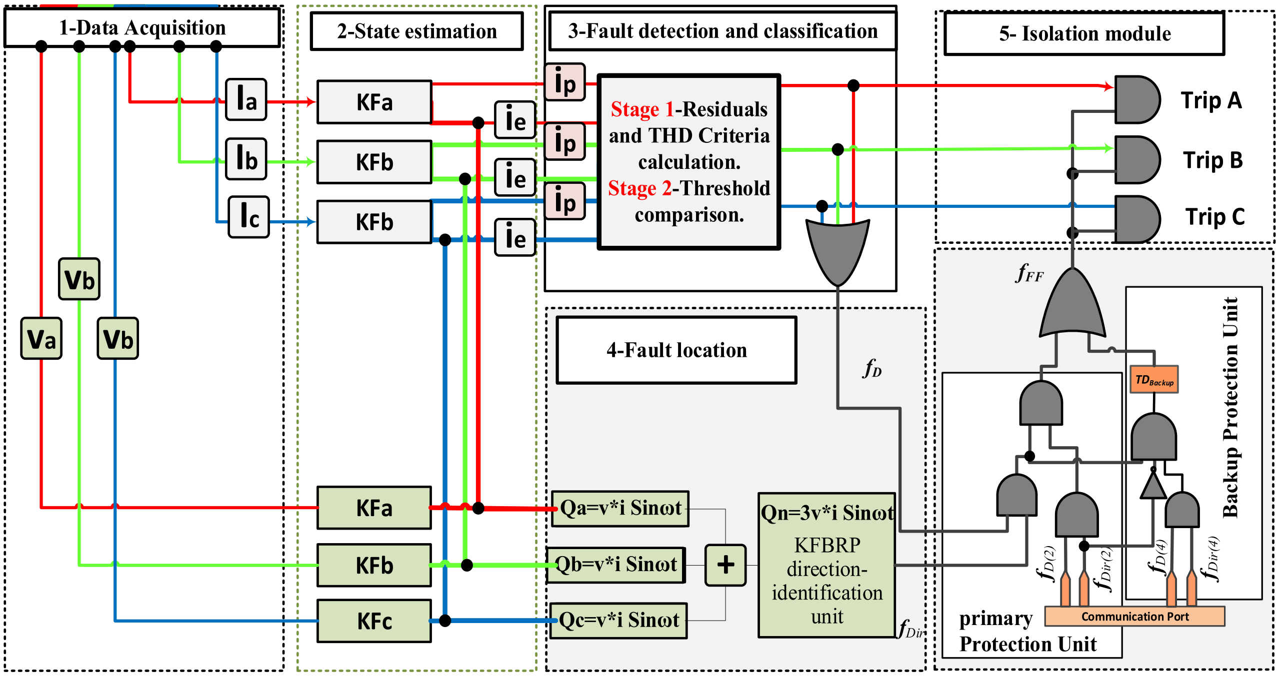

FIGURE 2. Schematic diagram of the proposed protection scheme.

communication-assisted fault-location module is employed to locate the faulty section of the microgrid in the proposed protection scheme. This module includes a direction identification unit, primary-protection unit, and backup-protection unit.

1) KFBRP DIRECTION IDENTIFICATION UNIT

The KFBRF direction identification unit employs the directional characteristics of KF-based reactive power to determine the fault direction. The third harmonic component of the three-phase voltage and current signals is utilized to compute the KF-based reactive power in any section. The three-phase KFBRP will be less than zero in case of forward faults, and greater than zero for the reverse faults.

2) PRIMARY AND BACKUP-PROTECTION UNITS

Several relays may see a fault in a particular zone as a forward/reverse fault. Therefore, the three adjacent relays communicate among themselves to identify the exact faulty distribution line. The use of the communication link among relays improves selectivity and avoids false tripping.

Each relay in the proposed scheme is equipped with a primary-protection unit and a backup-protection unit. The primary-protection unit operates immediately if a fault hits the primary-protection zone of the relay. However, when a fault occurs in the backup-protection zone of the relay, the backup-protection unit of a relay operates after a pre-defined time delay (TD_{Backup}). This time delay is introduced to permit the primary-protection units of the relays associated with the zone to operate first. Moreover, the sum of operating times of the primary-protection relay, and its corresponding circuit breaker must be less than chosen TD_{Backup}.

The fault-location logic of the proposed scheme has been shown in FIGURE 3. Relay R-1 is used to explain the fault-location procedure of the proposed scheme. The relay R-1 sends the fault-detection (f_D) and fault-direction (f_{Dir}) signals to two adjacent relays R-2 and R-4. At the same time, R-1 also gets both signals from the two adjacent relays. If R-1 detects a fault as a forward fault, then it checks the status of the fault by using the signals of the R-2. If the status of the fault at R-2 is forward, then the primary-protection zone is deemed to be faulty and a trip signal Q_{pz} is issued to the relevant circuit breakers. However, if the relay R-2 detects the fault as reverse then the relay R-2 looks at the status of fault at R-4. If the fault is identified as a forward fault by R-4, then the fault location is identified in the backup-protection zone and a tripping signal Q_{bz} is generated after a time delay TD_{Backup}. The primary-protection unit depends on the time delay TD_{Backup} to ensure that the relevant relays operate first. Finally, both the Q_{pz} and Q_{bz} are combined to generate a forward fault tripping signal f_{FF}. The trip signal f_{FF} is used in the fault isolation unit to isolate the faulty portion of the microgrid.

E. FAULT ISOLATION MODULE

After detecting, locating, and classifying the fault by the respective modules, the fault isolation module generates a trip signal based on the information received. The tripping signal will be transmitted to the subsequent circuit breaker of the faulty section to clear the fault.

IV. MICROGRID TEST MODEL

An IEC Microgrid test model (MTM) has been simulated in MATLAB/Simulink software to test the effectiveness of the proposed scheme. The single line diagram of the MTM

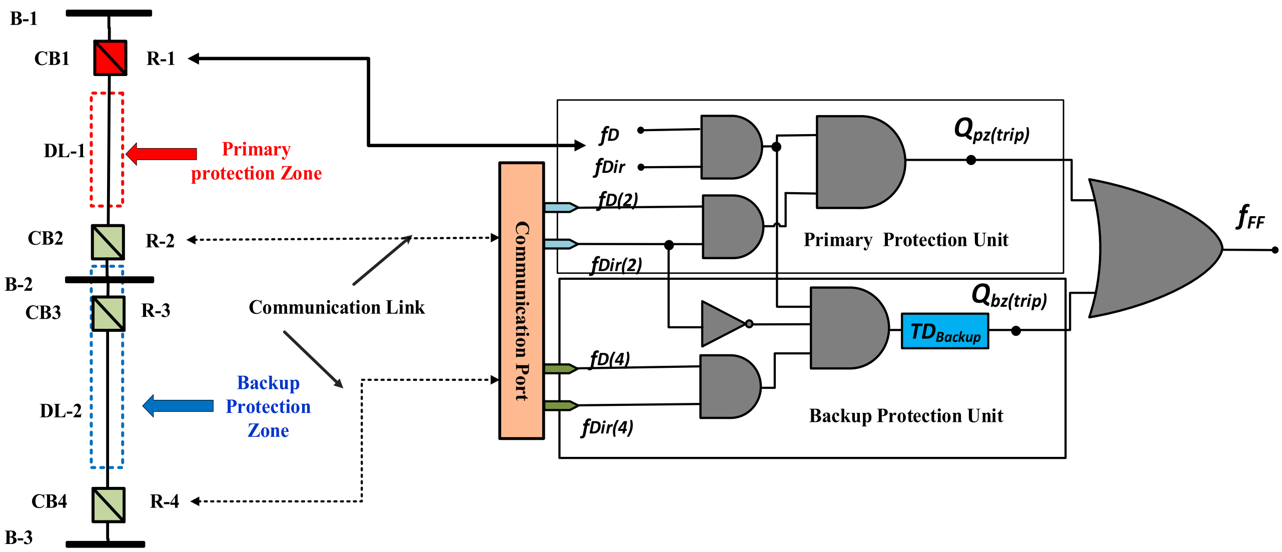

FIGURE 3. Fault zone identification logic diagram of proposed scheme R-1 under consideration.

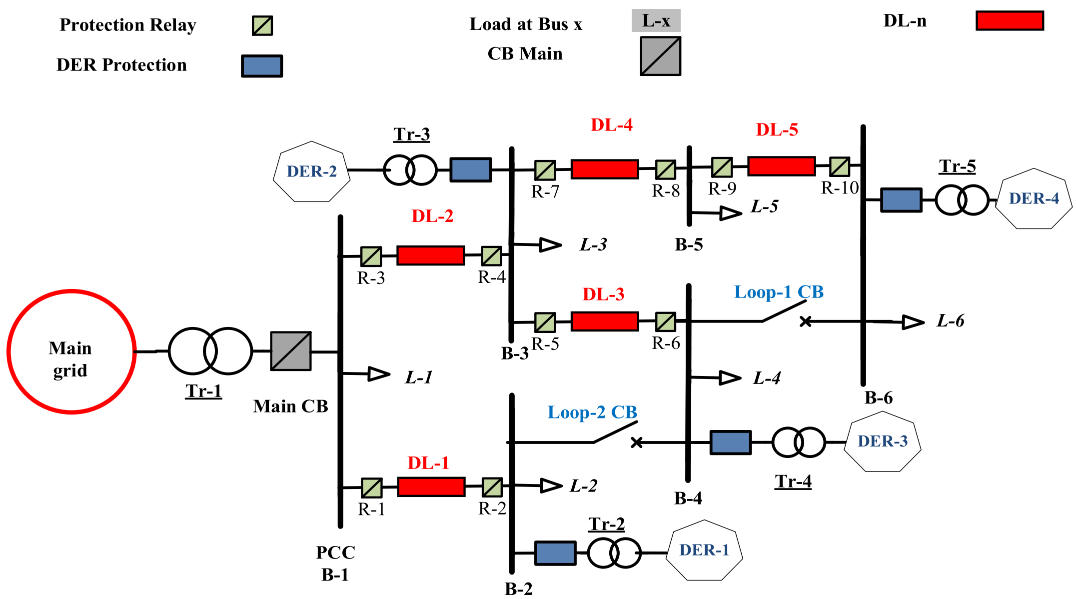

FIGURE 4. Standard International electro-technical commission IEC microgrid test model MTM.

is shown in FIGURE 4. The MTM consists of six buses, five distribution lines, three IIDERs, and one SDER. Each DER is connected to the microgrid test model by using step-up transformers. The main CB is worked to transform the operating mode of the MTM from grid-tied or autonomous mode and vice versa. The remaining two circuit breakers, loop-1 CB and loop-2 CB are used to operate the MTM in radial, and looped topological structures. The network and load parameters of the MTM are acquired from [36].

V. SIMULATION RESULTS

To verify the usefulness of the proposed protection scheme, a detailed fault analysis was performed on the MTM. In the fault analysis, all ten types of short circuit faults, which include three-phase faults, line-to-line, double line to ground faults (DLG) faults, and single-line-to-ground (SLG) faults were considered in both grid-tied and autonomous modes of operation. To validate the efficiency of the proposed scheme against HIFs, the HIFs were also simulated for all ten types of faults.

A. AUTONOMOUS MODE OF OPERATION

To validate the efficacy of the proposed scheme for solid faults in the autonomous mode of operation, a solid ACG fault has been simulated at DL-5 of the MTM at 50% of total line length with loop-1 CB open and loop-2 CB closed. The three-phase current, residuals, THDs, and KFBRP at the R-9 in the

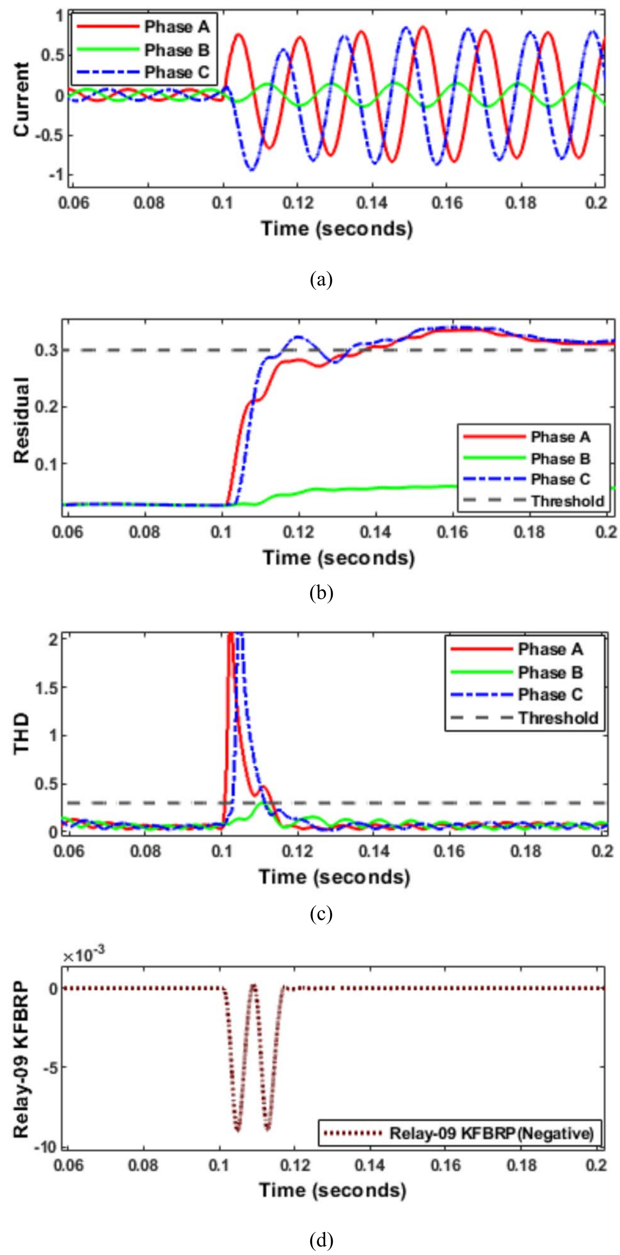

FIGURE 5. A DLG fault occur at DL-5 of MTM in autonomous mode with a resistance of 0.01 ohms.

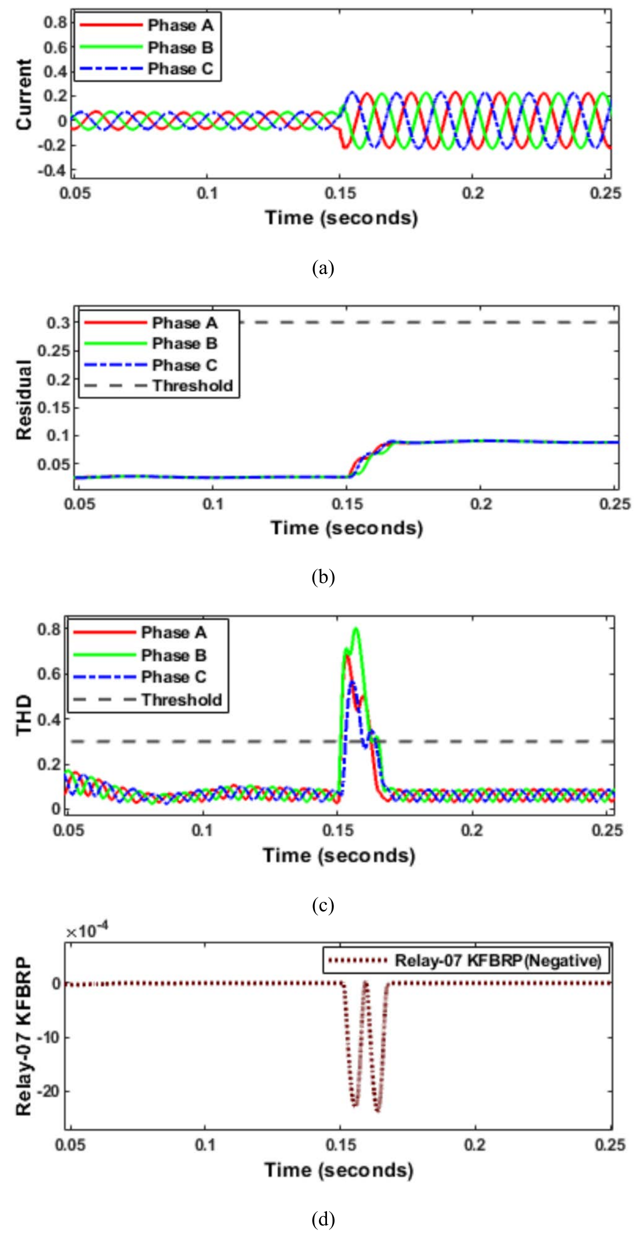

FIGURE 6. A TPG fault occurs at DL-4 of MTM in autonomous mode with a resistance of 75 ohms.

MTM are shown in FIGURE 5. FIGURE 5 indicates that the THD of phases A and C are higher than the threshold value of 0.3, whereas the THD of phase B is significantly smaller than the threshold value. However, although the residuals exceed the threshold, it happens so late that they do not serve as an adequate criterion in this case. Nevertheless, since the fault-detection decision is also based on THD, the scheme successfully detects this fault, even though the current is low due to autonomous mode. This demonstrates the key role of dual criterion for detection as well as classification of faults in the autonomous mode. Furthermore, at relay-9, the negative value of reactive power in each phase confirms the presence of a forward fault in section DL-5.

A high impedance ABCG fault, with a resistance of 75 ohms, is considered at DL-4 of MTM at 20% of total line length to verify the effectiveness of the scheme against HIFs in autonomous mode. For this case, loop-1 CB and loop-2 CB were closed. The three-phase current, residuals, THDs, and KFBRP at R-7 in the MTM are shown in FIGURE 6. Although the residuals are not able to detect this HIF fault in autonomous mode, however, the THD can detect it. Note that HIF in autonomous mode leads to very low fault currents, consequently, the residuals cannot sense the fault. Nevertheless, the THD successfully detects this fault under challenging conditions. This verifies the effectiveness of the proposed dual criteria for fault detection. Moreover, the

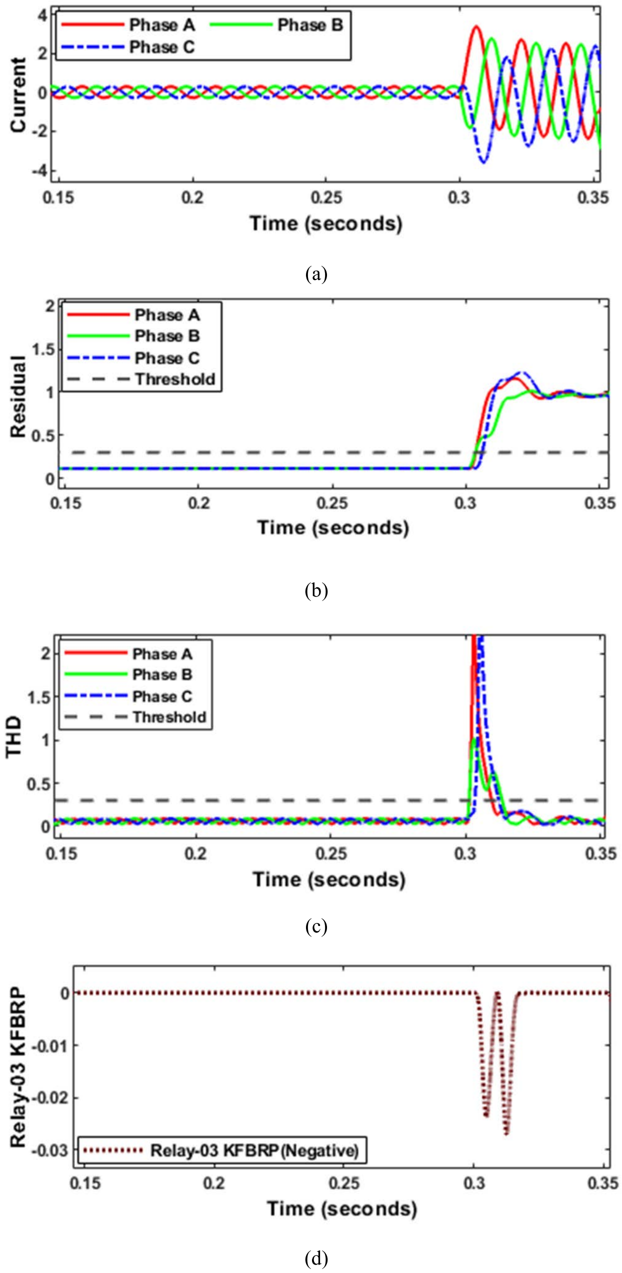

FIGURE 7. A TP fault occurs at DL-2 of MTM in grid-tied mode with a resistance of 0.01 ohms.

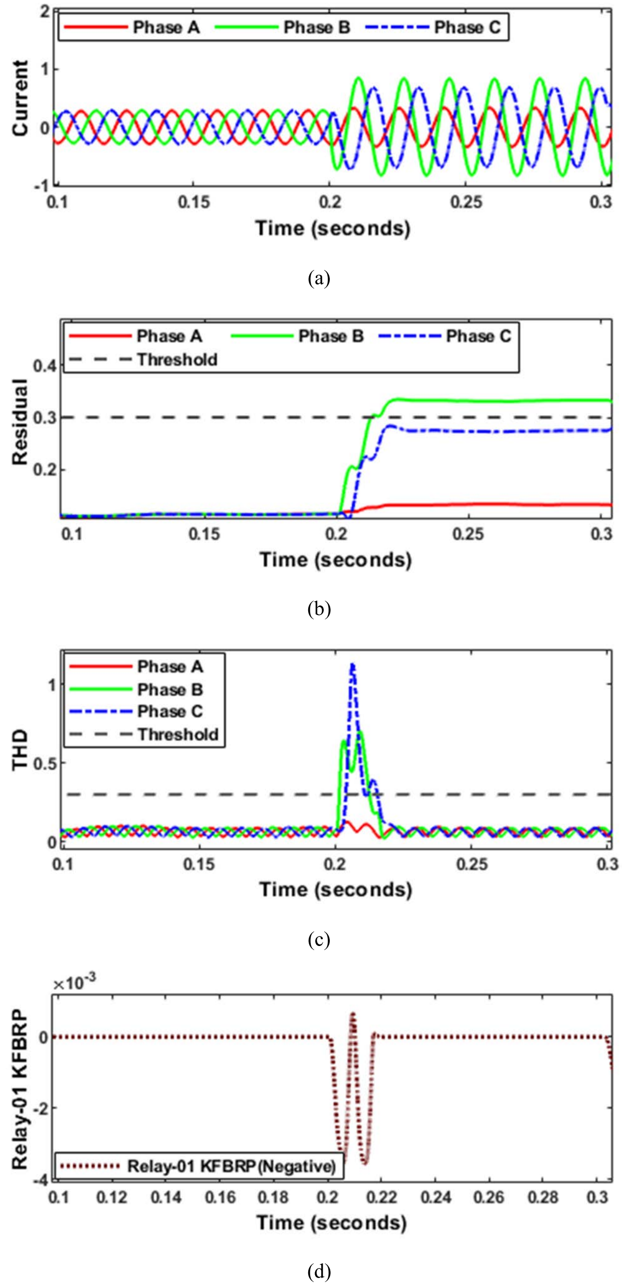

FIGURE 8. A BCG fault occurs at DL-1 of MTM in grid-tied mode with a resistance of 45 ohms.

negative value of three-phase KFBRP at relay R-7 indicates the presence of a forward fault in section DL-4.

B. GRID-TIED MODE OF OPERATION

This case is intended to validate the proposed protection scheme for grid-tied operation. To validate the effectiveness in grid-tied mode, a solid three-phase fault at DL-2 of MTM at 10% of total line length in the grid-tied mode of operation is simulated. The three-phase currents, the residuals, THDs, and the KFBRP for the fault are illustrated in FIGURE 7. It is clear from FIGURE 7 that both the residual and THD of all three phases are higher as compared to the threshold value. Therefore, the effectiveness of the proposed fault-detection criteria in the grid-tied case is verified. The negative value of KFBRP at R-3 in the MTM indicates the presence of the forward fault in section DL-2.

To verify the proposed scheme against HIF in grid-tied mode, let us assume a high impedance BCG fault hits the DL-1 of the MTM at 80% of total line length in grid-tide mode with a resistance of 45 ohms. The three-phase currents, the residuals, the THDs, and the KFBRP for this case study are shown in FIGURE 8. FIGURE 8 clearly illustrates that

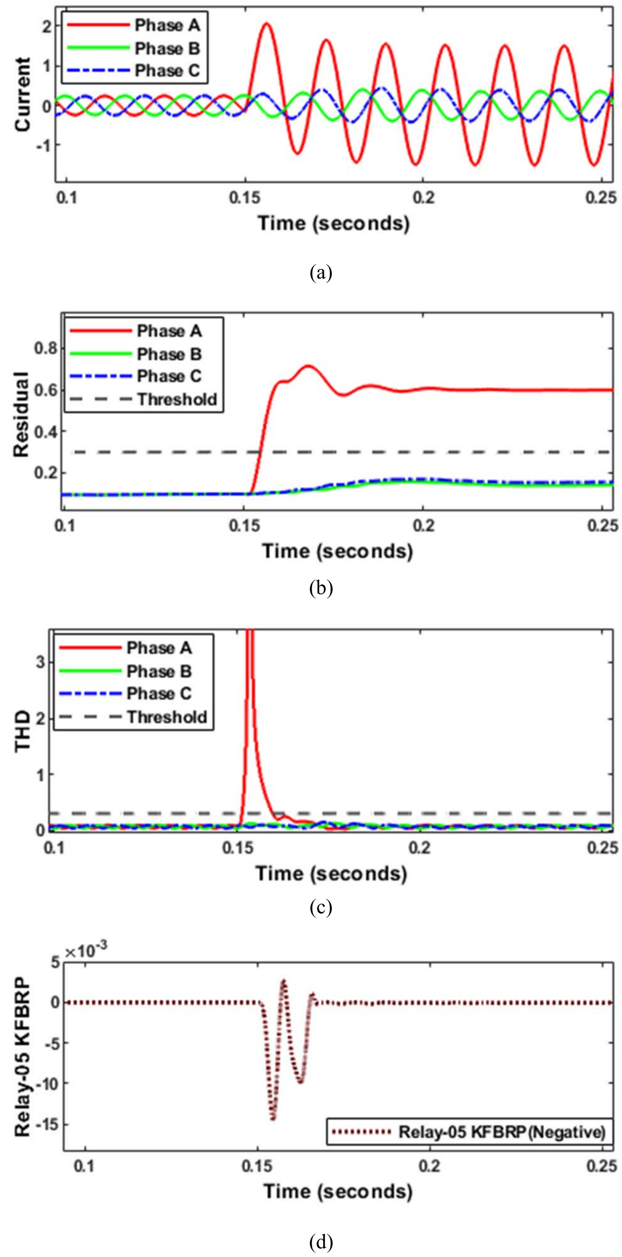

FIGURE 9. An AG fault with a resistance of 0.01 ohms occurs at DL-3 of MTM in grid-tied mode.

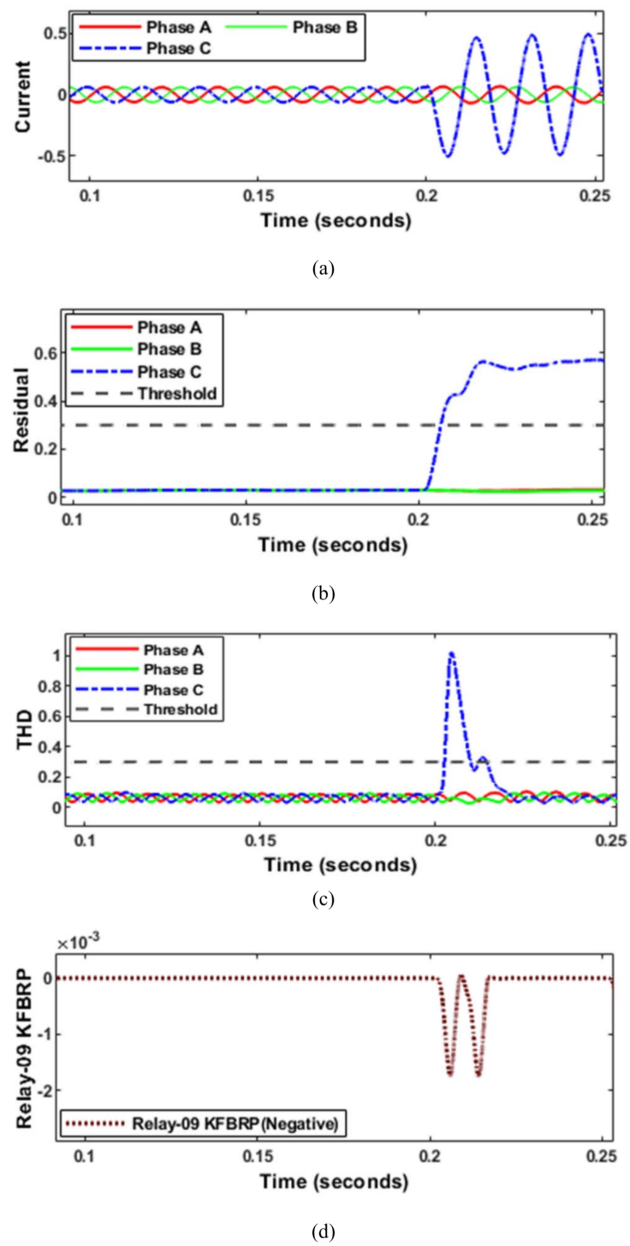

FIGURE 10. A CG fault simulated at DL-5 of MTM in autonomous mode with a resistance of 20 ohms.

the THD is useful for the HIF fault-detection in this case also. Hence, the KFBRP for this case is less than zero, which indicates the presence of a forward fault at DL-1.

C. SINGLE-PHASE FAULTS

The most common faults in the power system are single-phase by nature. Therefore, the proposed protection scheme is also tested against SLG faults in autonomous as well as grid-tied modes. For this, an AG fault was simulated at DL-3 of the MTM at 30% of the total line length in the grid-tied operational mode. The currents, residuals, THDs, and KFBRP at R-5 in MTM are shown in FIGURE 9 which indicates that the single-phase fault is successfully detected and located by the proposed scheme.

To test the proposed scheme against single-phase HIF, a high impedance CG fault at DL-5 of the MTM at 60% of total line length in autonomous mode was simulated. The currents, residuals, THDs, and KFBRP at the R-9 are shown in FIGURE 10. FIGURE 10 indicates the successful operation of the proposed scheme. The proposed protection scheme can protect single-phase solid as well as the HIF faults.

D. OPERATION TIMES OF PROPOSED KF-BASED SCHEME

Conclusively, from the results of all case studies of the proposed scheme, it has been observed that all faults are detected

TABLE 1. The internal operation time-period (TP_{op}(ms)) for the proposed method under different scenarios.

Microgrid-topologies	DL-N	Fault location	Grid-tied mode			Autonomous mode			Single-phase faults		
		($F_{L,Km}$)	Fault type	($R_{f,ohm}$)	TP_{op}(ms)	Fault type	($R_{f,ohm}$)	TP_{op}(ms)	Fault type	($R_{f,ohm}$)	TP_{op}(ms)
Radial	DL-3	10	A-G	0	10.26	AB	20	11.22	A-G	0.01	10.21
	DL-1	20	BC-G	45	14.97	BC-G	30	10.21	C-G	30	14.17
	DL-2	30	ABC-G	0	13.15	ABC	50	14.26	B-G	0	10.22
Meshed	DL-5	10	C-G	20	10.18	AC-G	0	10.22	C-G	20	11.25
	DL-3	20	B-G	0	14.17	AB	20	13.25	B-G	0	13.35
	DL-4	30	ABC	60	10.22	ABC-G	75	13.30	A-G	30	10.01

TABLE 2. Comparison with other similar existing schemes.

Parameters	Existing microgrid protection schemes						Proposed scheme
	EEMD based scheme	MM based scheme	FL based scheme	HT Based scheme	TKEO based scheme	ST Based scheme	
Accuracy %	85.20	64.27	88.96	69.96	96.49	89.2	91.6
Internal operation time (ms)	80 m sec on average	Less than 18 m sec	Less than 75 m sec	Less than 23 m sec	10 m sec on average	Less than 18 m sec	Less than 15 m sec
Robustness in different modes	Yes	No	No	No	Yes	Yes	Yes
Threshold Adjustment requirement	No	Yes	Yes	Yes	No	Yes	No
Computation burden	Moderate	Low	Moderate	Moderate	Very low	Low	Very low
Implementation Cost	Low	Low	Low	Moderate	Moderate	Low	Very low
Noise Consideration	No	Yes	No	No	No	Yes	Yes

by the primary-protection unit, within half a cycle (<15 ms). The internal operation times for representative cases of the KF-based proposed scheme are presented in Table 1. Note that the corresponding CB needs 2.5 additional cycles to separate the faulty portion from the healthy microgrid.

VI. COMPARISON WITH OTHER SCHEMES

Some other similar existing microgrid protection schemes, listed in Table 2, are compared to a large extent with the proposed KF-based scheme for a fair judgment. Firstly, all the other existing schemes are described briefly;

A. ENSEMBLE EMPIRICAL MODE DECOMPOSITION (EEMD) BASED SCHEME

The first scheme utilized EEMD on the current signal of the considered bus to compute spectral differential energy (SDE) for effective fault detection in AC microgrids [37]. The SDE is compared with the relay threshold setting for a decision on fault detection. In addition, this proposed scheme covers both grid-tied and, islanded modes.

B. MATHEMATICAL MORPHOLOGY (MM) BASED SCHEME

This scheme used mathematical morphology (MM) for microgrid protection [38]. Initially, the scheme implements a dilation and erosion median filter on the current signal for the detection as well as classification of faults. At last, the recursive least square (LS) method was used for the section identification in microgrids.

C. FUZZY LOGIC (FL) BASED SCHEME

This scheme was based on interval-type two (IT-2) fuzzy logic systems for reliable protection of microgrid. However, two different fuzzy systems are deployed for the detection, classification, and locating of faults in microgrids [24].

D. HILBERT-TRANSFORM (HT) BASED SCHEME

Furthermore, this scheme in [20], used Hilbert-transform to compute the superimposed component. The sequence components of superimposed currents are utilized for fault detection. However, the directional properties of superimposed reactive energy components are utilized for fault classification and location in microgrids with certain threshold settings.

E. TEAGER-KAISER ENERGY OPERATOR (TKEO) BASED SCHEME

TKEO was implemented in [19] on the measured current signature for reliable protection of microgrid. However, the squared sum of three-phase currents (SSC) was used for the detection of fault in this scheme, while SC_a, SC_b, SC_c of individual phases were used for the fault classification.

F. S-TRANSFORM (ST) BASED SCHEME

In [39] S-transform was used on the current signal at both ends to calculate differential energy for the detection of faults in microgrids. In addition, maximum amplitude curve was used to classify the faulty events.

In summary, the comparison of all the above schemes was carried out for critical parameters including: (i) internal operating time; (ii) robustness during different modes, (iii) threshold adjustment requirement, (iv) computation burden, (v) cost of implementation, (vi) fault detection accuracy; and (vii) noise consideration. The comparative analysis in Table 2 demonstrates that, in terms of both accuracy and internal operation time, only the TKEO-based scheme is marginally superior compared to the proposed KF-based scheme. Nevertheless, the proposed KF-based scheme offers additional advantages of noise consideration and a very low implementation cost as compared to the TKEO-based scheme.

VII. CONCLUSION

Microgrids are small distribution networks that can be operated in grid-tied and autonomous modes to resolve power quality and reliability issues. However, microgrid operation is associated with protection and control challenges. This paper proposed a new protection scheme for Microgrids using KF. KF-based dual criteria were developed for fault detection and classification. Moreover, the directional characteristics of KF-based reactive power were obtained from third harmonic components of three-phase voltage and currents to locate the faulty part in the microgrids. Extensive simulations using a Simulink model of the proposed strategy proved its effectiveness. The proposed strategy is fast, simple, cost-effective, and has a low computational burden. Further studies for unbalanced microgrid conditions were to be under consideration for future work, and also the communication less Kalman Filter-Based microgrid protection scheme is also left as future work.

APPENDIX

KF approach

1. Put primary estimates for the state vector and its matrix of covariance ($\hat{X}_n^- and \hat{P}_n^-$)
2. Determine the Kalman gain at instant n by $KG_n = (\frac{P_n^- H}{H^T P_n^- H} + r_n)$
3. m At nth instant, the estimation is updated through the measurements
4. $\hat{X}_n^+ \doteq X_n^- + KG_n(y_n - H^T X_n^-)$
   where;
   $$q_n \doteq E\left\{w_n^2\right\}, r_n \doteq E\left\{u_n^2\right\}$$
   From observation y_1 to y_{n-1} prior estimates of a state vector X_n in nth instant is
   $$\hat{X}_n^- = \hat{E}\left\{X_n \,|\, y_{n-1}, \ldots .y_n\right\}$$
   And after using nth observation posterior estimates of a state vector X_n is
   $$\hat{X}_n^+ = \hat{E}\left\{X_n \,|\, y_n, \ldots .y_1\right\}$$
5. Determine error of covariance for improved estimated with
   $$P_n^+ = P_n^- KG_n H^T P_n^-$$
6. Then Kalman filter block accurately calculates
   $$P_n^+ = P_n^- KG_n H^T P_n^- \hat{X}_{n+1} = A_n \hat{X}_n$$
   $$\hat{P}_{n+1} = A_n P_n^+ A_n^T + q_n bb^T$$
7. Then start from step 2

REFERENCES

[1] D. Liu, D. Tzelepis, and A. Dysko, "Protection of microgrids with high amounts of renewables: Challenges and solutions," in *Proc. 54th Int. Universities Power Eng. Conf. (UPEC)*, Sep. 2019, pp. 2–7, doi: 10.1109/UPEC.2019.8893485.

[2] B. Wang and L. Jing, "A protection method for inverter-based microgrid using current-only polarity comparison," *J. Modern Power Syst. Clean Energy*, vol. 8, no. 3, pp. 446–453, 2020, doi: 10.35833/MPCE.2018.000722.

[3] N. K. Sharma and S. R. Samantaray, "PMU assisted integrated impedance angle-based microgrid protection scheme," *IEEE Trans. Power Del.*, vol. 35, no. 1, pp. 183–193, Feb. 2020, doi: 10.1109/TPWRD.2019.2925887.

[4] B. Mahamedi and J. E. Fletcher, "Trends in the protection of inverter-based microgrids," *IET Gener. Transm. Distrib.*, vol. 13, pp. 4511–4522, Oct. 2019, doi: 10.1049/iet-gtd.2019.0808.

[5] A. A. Memon and K. Kauhaniemi, "A critical review of AC microgrid protection issues and available solutions," *Electr. Power Syst. Res.*, vol. 129, pp. 23–31, Dec. 2015, doi: 10.1016/j.epsr.2015.07.006.

[6] B. J. Brearley and R. R. Prabu, "A review on issues and approaches for microgrid protection," *Renew. Sustain. Energy Rev.*, vol. 67, no. 1, pp. 988–997, 2017, doi: 10.1016/j.rser.2016.09.047.

[7] A. Oudalov and A. Fidigatti, "Adaptive network protection in microgrids," *ABB Int. J. Distrib. Energy Resour.*, vol. 5, pp. 201–227, 2009.

[8] F. Coffele, C. Booth, and A. Dysko, "An adaptive overcurrent protection scheme for distribution networks," *IEEE Trans. Power Del.*, vol. 30, no. 2, pp. 561–568, Apr. 2015, doi: 10.1109/TPWRD.2013.2294879.

[9] M. S. Elbana, N. Abbasy, A. Meghed, and N. Shaker, "μPMU-based smart adaptive protection scheme for microgrids," *J. Modern Power Syst. Clean Energy*, vol. 7, no. 4, pp. 887–898, Jul. 2019, doi: 10.1007/s40565-019-0533-6.

[10] R. Jain, D. L. Lubkeman, and S. M. Lukic, "Dynamic adaptive protection for distribution systems in grid-connected and islanded modes," *IEEE Trans. Power Del.*, vol. 34, no. 1, pp. 281–289, Feb. 2019, doi: 10.1109/TPWRD.2018.2884705.

[11] R. Sitharthan, M. Geethanjali, and T. K. S. Pandy, "Adaptive protection scheme for smart microgrid with electronically coupled distributed generations," *Alexandria Eng. J.*, vol. 55, no. 3, pp. 2539–2550, Sep. 2016, doi: 10.1016/j.aej.2016.06.025.

[12] S. F. Zarei, H. Mokhtari, and F. Blaabjerg, "Fault detection and protection strategy for islanded inverter-based microgrids," *IEEE J. Emerg. Sel. Topics Power Electron.*, vol. 9, no. 1, pp. 472–484, Feb. 2021, doi: 10.1109/JESTPE.2019.2962245.

[13] S. Ranjbar, A. R. Farsa, and S. Jamali, "Voltage-based protection of microgrids using decision tree algorithms," *Int. Trans. Electr. Energy Syst.*, vol. 30, no. 4, pp. 1–15, Apr. 2020, doi: 10.1002/2050-7038.12274.

[14] P. T. Manditereza and R. C. Bansal, "Protection of microgrids using voltage-based power differential and sensitivity analysis," *Int. J. Electr. Power Energy Syst.*, vol. 118, Jun. 2020, Art. no. 105756, doi: 10.1016/j.ijepes.2019.105756.

[15] J. O. C. P. Pinto and M. Moreto, "Protection strategy for fault detection in inverter-dominated low voltage AC microgrid," *Electr. Power Syst. Res.*, vol. 190, Jan. 2021, Art. no. 106572, doi: 10.1016/j.epsr.2020.106572.

[16] A. Soleimanisardoo, H. K. Karegar, and H. H. Zeineldin, "Differential frequency protection scheme based on off-nominal frequency injections for inverter-based islanded microgrids," *IEEE Trans. Smart Grid*, vol. 10, no. 2, pp. 2107–2114, Mar. 2019, doi: 10.1109/TSG.2017.2788851.

[17] S. Baloch, S. Z. Jamali, K. K. Mehmood, S. B. A. Bukhari, M. S. U. Zaman, A. Hussain, and C.-H. Kim, "Microgrid protection strategy based on the autocorrelation of current envelopes using the squaring and low-pass filtering method," *Energies*, vol. 13, no. 9, p. 2350, May 2020, doi: 10.3390/en13092350.

[18] O. A. Gashteroodkhani, M. Majidi, M. S. Fadali, M. Etezadi-Amoli, and E. Maali-Amiri, "A protection scheme for microgrids using time-time matrix z-score vector," *Int. J. Electr. Power Energy Syst.*, vol. 110, pp. 400–410, Sep. 2019, doi: 10.1016/j.ijepes.2019.03.040.

[19] M. A. Jarrahi, H. Samet, and T. Ghanbari, "Novel change detection and fault classification scheme for AC microgrids," *IEEE Syst. J.*, vol. 14, no. 3, pp. 3987–3998, Sep. 2020, doi: 10.1109/JSYST.2020.2966686.

[20] S. B. A. Bukhari, M. S. U. Zaman, R. Haider, Y.-S. Oh, and C.-H. Kim, "A protection scheme for microgrid with multiple distributed generations using superimposed reactive energy," *Int. J. Electr. Power Energy Syst.*, vol. 92, pp. 156–166, Nov. 2017, doi: 10.1016/j.ijepes.2017.05.003.

[21] H.-C. Seo, ‘‘New protection scheme based on coordination with tie switch in an open-loop microgrid,’’ *Energies*, vol. 12, no. 24, p. 4756, Dec. 2019, doi: 10.3390/en12244756.

[22] S. Mirsaeidi, D. M. Said, M. W. Mustafa, and M. H. Habibuddin, ‘‘A protection strategy for micro-grids based on positive-sequence component,’’ *IET Renew. Power Gener.*, vol. 9, no. 6, pp. 600–609, Aug. 2015, doi: 10.1049/iet-rpg.2014.0255.

[23] S. Mirsaeidi, D. M. Said, M. W. Mustafa, M. H. Habibuddin, and K. Ghaffari, ‘‘Fault location and isolation in micro-grids using a digital central protection unit,’’ *Renew. Sustain. Energy Rev.*, vol. 56, pp. 1–17, Apr. 2016, doi: 10.1016/j.rser.2015.10.162.

[24] S. B. A. Bukhari, R. Haider, M. S. U. Zaman, Y.-S. Oh, G.-J. Cho, and C.-H. Kim, ‘‘An interval type-2 fuzzy logic based strategy for microgrid protection,’’ *Int. J. Electr. Power Energy Syst.*, vol. 98, pp. 209–218, Jun. 2018, doi: 10.1016/j.ijepes.2017.11.045.

[25] O. A. Gashteroodkhani, M. Majidi, and M. Etezadi-Amoli, ‘‘A combined deep belief network and time-time transform based intelligent protection scheme for microgrids,’’ *Electr. Power Syst. Res.*, vol. 182, May 2020, Art. no. 106239, doi: 10.1016/j.epsr.2020.106239.

[26] J. J. Q. Yu, Y. Hou, A. Y. S. Lam, and V. O. K. Li, ‘‘Intelligent fault detection scheme for microgrids with wavelet-based deep neural networks,’’ *IEEE Trans. Smart Grid*, vol. 10, no. 2, pp. 1694–1703, Mar. 2019.

[27] D. P. Mishra, S. R. Samantaray, and G. Joos, ‘‘A combined wavelet and data-mining based intelligent protection scheme for microgrid,’’ *IEEE Trans. Smart Grid*, vol. 7, no. 5, pp. 2295–2304, Sep. 2016, doi: 10.1109/TSG.2015.2487501.

[28] S. Beheshtaein, R. Cuzner, M. Savaghebi, S. Golestan, and J. M. Guerrero, ‘‘Fault location in microgrids: A communication-based high-frequency impedance approach,’’ *IET Gener., Transmiss. Distrib.*, vol. 13, no. 8, pp. 1229–1237, Apr. 2019, doi: 10.1049/iet-gtd.2018.5166.

[29] M. Manohar, E. Koley, S. Ghosh, D. K. Mohanta, and R. C. Bansal, ‘‘Spatio-temporal information based protection scheme for PV integrated microgrid under solar irradiance intermittency using deep convolutional neural network,’’ *Int. J. Electr. Power Energy Syst.*, vol. 116, Mar. 2020, Art. no. 105576, doi: 10.1016/j.ijepes.2019.105576.

[30] S. B. A. Bukhari, C. Kim, K. K. Mehmood, R. Haider, and M. Saeed Uz Zaman, ‘‘Convolutional neural network-based intelligent protection strategy for microgrids,’’ *IET Gener., Transmiss. Distrib.*, vol. 14, no. 7, pp. 1177–1185, Apr. 2020, doi: 10.1049/iet-gtd.2018.7049.

[31] R. Haider, C. H. Kim, T. Ghanbari, and S. B. A. Bukhari, ‘‘Harmonic-signature-based islanding detection in grid-connected distributed generation systems using Kalman filter,’’ *IET Renew. Power Gener.*, vol. 12, no. 15, pp. 1813–1822, Nov. 2018, doi: 10.1049/iet-rpg.2018.5381.

[32] T. Ghanbari, ‘‘Kalman filter based incipient fault detection method for underground cables,’’ *IET Gener., Transmiss. Distrib.*, vol. 9, no. 14, pp. 1988–1997, Nov. 2015, doi: 10.1049/iet-gtd.2015.0040.

[33] M. M. Rana, L. Li, and S. W. Su, ‘‘Microgrid state estimation and control using Kalman filter and semidefinite programming technique,’’ *Int. Energy J.*, vol. 16, no. 2, pp. 47–56, 2016.

[34] P. Shaw and M. K. Jena, ‘‘A novel event detection and classification scheme using wide-area frequency measurements,’’ *IEEE Trans. Smart Grid*, vol. 12, no. 3, pp. 2320–2330, May 2021, doi: 10.1109/TSG.2020.3039274.

[35] A. Jalilian, M. T. Hagh, and S. M. Hashemi, ‘‘An innovative directional relaying scheme based on postfault current,’’ *IEEE Trans. Power Del.*, vol. 29, no. 6, pp. 2640–2647, Dec. 2014, doi: 10.1109/TPWRD.2014.2312019.

[36] S. Kar, S. R. Samantaray, and M. D. Zadeh, ‘‘Data-mining model based intelligent differential microgrid protection scheme,’’ *IEEE Syst. J.*, vol. 11, no. 2, pp. 1161–1169, Jun. 2017.

[37] A. Anand and S. Affijulla, ‘‘Ensemble empirical mode decomposition-based differential protection scheme for islanded and grid-tied AC microgrid,’’ *IET Gener., Transmiss. Distrib.*, vol. 14, no. 26, pp. 6674–6681, Dec. 2020, doi: 10.1049/iet-gtd.2020.1117.

[38] T. Gush, S. B. A. Bukhari, R. Haider, S. Admasie, Y.-S. Oh, G.-J. Cho, and C.-H. Kim, ‘‘Fault detection and location in a microgrid using mathematical morphology and recursive least square methods,’’ *Int. J. Electr. Power Energy Syst.*, vol. 102, pp. 324–331, Nov. 2018, doi: 10.1016/j.ijepes.2018.04.009.

[39] A. Langarizadeh and S. Hasheminejad, ‘‘A new differential algorithm based on S-transform for the micro-grid protection,’’ *Electr. Power Syst. Res.*, vol. 202, Jan. 2022, Art. no. 107590, doi: 10.1016/j.epsr.2021.107590.

FAISAL MUMTAZ received the B.S. degree in electrical engineering power from the University of Wah, Wah Cantt, Pakistan, in 2015, and the M.S. degree in electrical engineering power from the U.S. Pakistan Center for Advanced Studies in Energy, National University of Sciences and Technology (NUST), Islamabad, Pakistan, in 2021, where he is currently pursuing the Ph.D. degree. From 2017 to 2018, he was an Instructor at the Electrical Engineering Department, Swedish Institute of Science and Technology, Wah Cantt. He was also awarded USAID fully funded scholarship for his master's degree. His research interests include microgrids protection, state estimation, distributed generation, discrete signal processing, and system identification.

KASHIF IMRAN received the B.Sc. and M.Sc. degrees in electrical engineering from the University of Engineering and Technology (UET) Lahore, in 2006 and 2008, respectively, and the Ph.D. degree in electrical engineering from the University of Strathclyde, in 2015. He has worked at the Transmission and Distribution Division, SIEMENS, and the Power Distribution Design Section, NESPAK, from 2006 to 2007. He was a Faculty Member at the University of Engineering and Technology (UET) Lahore and COMSATS University Lahore. He was the Inaugural Head of the Department of Electrical Power Engineering at the U.S. Pakistan Center for Advanced Studies in Energy, National University of Sciences and Technology, Islamabad, from 2018 to 2021. His research interests include energy policy, optimization for power systems and electricity markets operations and planning, and power system protection. He received the Commonwealth Scholarship for his Ph.D. degree.

SYED BASIT ALI BUKHARI received the master's degree in electrical power engineering from the University of Engineering and Technology, Taxila, Pakistan, and the Ph.D. degree in electrical power engineering from Sungkyunkwan University, South Korea. He is currently an Assistant Professor with the Department of Electrical Engineering, The University of Azad Jammu and Kashmir, Muzaffarabad, Pakistan. His research interests include voltage stability, distributed generation, smart grids, power system modeling, power system planning, microgrids, multi-microgrids, and virtual power plants.

KHAWAJA KHALID MEHMOOD received the B.Sc. degree in electrical engineering from the Mirpur University of Science and Technology, Mirpur, Pakistan, in 2012, and the M.Sc. and Ph.D. degrees in electrical engineering from Sungkyunkwan University, South Korea, in 2015 and 2019, respectively. He is currently working as an Assistant Professor with the Department of Electrical Engineering, The University of Azad Jammu and Kashmir, Muzaffarabad, Azad Kashmir, Pakistan. His research interests include planning and operations of distribution systems, electric vehicles, and electrical energy storage systems.

ABDULLAH ABUSORRAH (Senior Member, IEEE) received the Ph.D. degree in electrical engineering from the University of Nottingham, U.K., in 2007. He is currently a Professor and the Head of the Center for Renewable Energy and Power Systems, in Department of Electrical and Computer Engineering, King Abdulaziz University, Jeddah, Saudi Arabia. His research interests include renewable energy, smart grid, the IoT, and system analysis.

MAQSOOD AHMAD SHAH received the B.Sc. degree in electrical engineering degree from the University of Engineering and Technology (UET), Taxila, in 2017, and the M.S. degree in electrical engineering (power) from the USPCAS-E, National University of Sciences and Technology (NUST), Islamabad, Pakistan, in 2021. He is currently working with HydroChina International Engineering (Pvt) Ltd., on the construction of a 60 MW wind power project in Pakistan. His research interests include of signal processing tools and machine learning applications in power system protection and control, DC microgrid, and suitable distribution networks for the integration of renewable energy resources (RERs) and electric vehicles.

SYED ALI ABBAS KAZMI received the bachelor's degree in electrical engineering from the University of Engineering and Technology, Taxila, Pakistan, the master's degree in electrical power engineering from the University of Engineering and Technology, Peshawar, Pakistan, and the Ph.D. degree in electrical power engineering from Sungkyunkwan University, South Korea. He is currently an Assistant Professor with the U.S. Pakistan Center for Advanced Studies in Energy, Department of Electrical Engineering, National University of Sciences and Technology. His research interests include voltage stability, distributed generation, smart grids, power system modeling, power system planning, microgrids, multi-microgrids, and virtual power plants.